Calcif Tissue Int
DOI 10.1007/s00223-012-9594-5

ORIGINAL RESEARCH

Arterial Microcalcification in Atherosclerotic Patients with and Without Chronic Kidney Disease: A Comparative High-Resolution Scanning X-Ray Diffraction Analysis

Dagmar-Christiane Fischer · Geert J. Behets · Oliver W. Hakenberg · Mathias Voigt · Benjamin A. Vervaet · Stef Robijn · Günther Kundt · Wolfgang Schareck · Patrick C. D'Haese · Dieter Haffner

Received: 26 October 2011 / Accepted: 14 March 2012

Abstract Vascular calcification, albeit heterogeneous in terms of biological and physicochemical properties, has been associated with ageing, lifestyle, diabetes, and chronic kidney disease (CKD). It is unknown whether or not moderately impaired renal function (CKD stages 2–4) affects the physiochemical composition and/or the formation of magnesium-containing tricalcium phosphate ($[Ca,Mg]_3[PO_4]_2$, whitlockite) in arterial microcalcification. Therefore, a high-resolution scanning X-ray diffraction analysis (European Synchrotron Radiation Facility, Grenoble, France) utilizing histological sections of paraffin-embedded arterial specimens derived from atherosclerotic patients with normal renal function ($n = 15$) and CKD (stages 2–4, $n = 13$) was performed. This approach allowed us to spatially assess the contribution of calcium phosphate (apatite) and whitlockite to arterial microcalcification. Per group, the number of samples (13 vs. 12) with sufficient signal intensity and total lengths of regions (201 vs. 232 μm) giving rise to diffractograms ("informative regions") were comparable. Summarizing all informative regions per group into one composite sample revealed calcium phosphate/apatite as the leading mineral phase in CKD patients, whereas in patients with normal renal function the relative contribution of whitlockite and calcium phosphate/apatite was on the same order of magnitude (CKD, calcium phosphate/apatite 157 μm, whitlockite 38.7 μm; non-CKD, calcium phosphate/apatite 79.0 μm, whitlockite 94.1 μm; each $p < 0.05$). Our results, although based on a limited number of samples, indicate that chronic impairment of renal function affects local magnesium homeostasis and thus contributes to the physicochemical composition of microcalcification in atherosclerotic patients.

Keywords Arterial microcalcification · Apatite · Chronic kidney disease · Whitlockite · X-ray diffraction · X-ray fluorescence

The authors have stated that they have no conflict of interest.

D.-C. Fischer (✉) · M. Voigt · D. Haffner
Department of Pediatrics, University Children's Hospital Rostock, Ernst-Heydemann-Str. 8, 18057 Rostock, Germany
e-mail: dagmar-christiane.fischer@med.uni-rostock.de

D.-C. Fischer · D. Haffner
Department of Pediatric Kidney, Liver and Metabolic Diseases, Hannover Medical School, Hannover, Germany

G. J. Behets · B. A. Vervaet · S. Robijn · P. C. D'Haese
Laboratory of Pathophysiology, University of Antwerp, Antwerp, Belgium

O. W. Hakenberg
Department of Urology, University of Rostock, Rostock, Germany

G. Kundt
Institute of Biostatistics and Informatics in Medicine, University of Rostock, Rostock, Germany

W. Schareck
Department of Vascular Surgery, University of Rostock, Rostock, Germany

Vascular calcification is among the (silent) symptoms of accelerated cardiovascular disease and, as such, contributes significantly to cardiovascular morbidity and mortality (for review see [1, 2] and references therein). Apart from ageing, lifestyle- and/or disease-related risk factors have been identified, e.g., hypertension, dyslipidemia, obesity, chronic kidney disease (CKD), and diabetes [3]. Intimal calcification is a common feature of advanced

Published online: 05 April 2012

atherosclerosis and develops almost exclusively in large and medium-sized conduit arteries. By contrast, the prevalence of media calcification increases with age, is in general higher in patients with CKD and/or diabetes, and is independent of atherosclerotic lesions [4, 5]. Media calcification can occur in arteries of any size and begins in matrix vesicles, followed by the formation of microcalcifications, which are likely to evolve over time into large calcific deposits [6].

Ectopic mineralization is an active and highly regulated process resembling several aspects of skeletal mineralization at the cellular and molecular levels rather than the uncontrolled, purely physicochemically based formation of an insoluble mineral phase [5, 7–11]. Apart from high extracellular phosphate and calcium concentrations, release of matrix vesicles from vascular smooth muscle cells, formation of apoptotic bodies, matrix remodeling, and the local and systemic concentrations of procalcific and anticalcific compounds contribute to vascular calcification [2, 4–10, 12–17].

Although mature calcifications are usually considered to be similar to bone, i.e. to consist of apatite ($Ca_{10}[PO_4]_6[OH]_2$), a magnesium-containing tricalcium phosphate ($[Ca,Mg]_3[PO_4]_2$, whitlockite) has been recognized in several pathological conditions [2, 18]. Among these are noninfectious and infectious dystrophic calcification, and whitlockite has been described in advanced media calcification in patients with end-stage renal disease [19–21]. Similarly, experiments in rats with chronic renal failure point to an association between high-dose calcitriol treatment and the formation of whitlockite [18]. It is currently not known whether such differences with respect to ultrastructural composition and the relative contributions of whitlockite and apatite are already present in media microcalcification. In fact, calcified arteries from patients with end-stage chronic renal failure have been investigated either after isolation of the mineral phase [19] or using synchrotron X-ray diffraction analysis with limited resolution (2×7 μm) [21]. Whereas with the former approach the information linking type and localization of the calcific deposit is lost, the latter is not suited for investigating microcalcification (<1 μm), which is considered to serve as a seed for subsequent calcification.

We used high-resolution (250×250 nm) scanning X-ray diffraction analysis at the European Synchrotron Radiation Facility (ESRF) in Grenoble, France, to investigate media microcalcification in arterial samples derived from patients with normal and moderately impaired renal function (CKD stages 2–4). To the best of our knowledge, such a high resolution cannot be achieved with Raman- and infrared spectroscopy, which are otherwise well suited for analyzing calcifications.

Methods

The study received appropriate ethics committee approval from the institutional review board in accordance with the Declaration of Helsinki, and all patients gave written informed consent. Adult patients with normal or impaired renal function undergoing elective vascular surgery (see below) were eligible for this study. Exclusion criteria included chronic infectious diseases (such as hepatitis, tuberculosis) and osteopetrosis.

A total of 28 patients were prospectively enrolled between September 2007 and August 2008. Tissue was sampled at the time of carotid endarterectomy for symptomatic or high-grade asymptomatic carotid stenosis ($n = 28$). Patients were categorized according to renal function, and an estimated glomerular filtration rate (eGFR) below 90 ml/min/1.73 m^2 (i.e., CKD stages 2–4) was used as a cut-off value. Demographic and clinical patient data are given in Table 1. The modification of diet in renal disease formula was used to calculate eGFR [22]. Clinical data were gathered by patient interview and/or review of charts. Enzyme-linked immunosorbent assays were used to determine fetuin-A (Epitope Diagnostics, San Diego, CA) and fibroblast growth factor-23 (FGF-23, C-terminal fragment; Immutopics, San Clemente, CA) as described [11]. No patients received 25-hydroxyvitamin D (cholecalciferol).

Specimen and Blood Samples

All tissue specimens were placed in 4 % buffered formalin and immediately transferred to the laboratory for further processing [18, 21]. Specimens taken during carotid endarterectomy were freed from surrounding tissue, and the calcified segment of the vessel was submitted to paraffin embedding without decalcification. The conditions of tissue fixation, i.e., source of buffered formalin, ratio tissue to fixative, and time of fixation, were kept constant throughout the study. Blood for determination of fetuin-A and FGF-23 was sampled at the time of surgery, aliquoted, and stored at –80 °C until further analysis.

Histochemical Analysis

Serial sections (4–5 μm) were prepared with a fully automated rotary microtome (RM 2255; Leica, Wetzlar, Germany). These sections were used for localization of calcific deposits by means of von Kossa (vK) staining in combination with Mayer's hemalum and eosin and simultaneous high-resolution scanning X-ray fluorescence and diffraction analysis (see below) [11, 18, 23]. Calcification was classified as described: powder-like distribution (shotgun-mineralization [microcalcification], vK1), confluent deposits

Table 1 Clinical characteristics and serum parameters of atherosclerotic patients with normal or reduced renal function at time of surgery

Parameter	All patients (17m/11f)	Normal renal function (7m/8f)	CKD stages 2–4 (10m/3f)	*p*
Age (years)	69 (46–88)	64 (46–88)	71 (59–82)	0.108
BMI (kg/m^2)	26.7 (20.6–47.7)	26.8 (20.6–47.7)	25.5 (22.9–33.8)	0.856
Hypertension (positive/negative)	25/3	13/2	12/1	1.000
Smoking history (positive/negative)	11/17	5/10	6/7	0.700
Pack-years	20 (10–40)	25 (20–35)	19 (10–40)	0.171
Diabetes (positive/negative)	13/15	7/8	6/7	1.000
HbA_{1c} (%)	6.6 (5.6–7.9)	6.8 (5.6–7.9)	6.4 (5.0–7.8)	0.905
Dyslipidemia (positive/negative)	21/7	11/4	10/3	1.000
LDL/HDL	2.1 (1.1–3.6)	1.71 (1.11–3.62)	2.10 (1.12–3.22)	0.235
Lipoprotein (a) (g/l)	0.18 (0.02–1.29)	0.15 (0.02–0.92)	0.27 (0.02–1.29)	0.295
Hematocrit (%)	0.4 0.29–0.45)	0.42 (0.32–0.45)	0.41 (0.29–0.45)	0.525
CRP (mg/l)	3.00 (1–16)	2.39 (1–15.1)	4.50 (1–16)	0.545
Creatinine (μmol/l)	80.3 (37.7–292)	64.3 (37.7–81.3)	121 (83.6–292)	<0.001
eGFR (ml/min/1.73 m^2)	97 (25–157)	125 (89.1–157)	59.1 (24.9–80.4)	<0.001

The median together with minimum and maximum is given

(vK2), confluent deposits plus at least one large destructive lesion (vK3), and ubiquitously distributed, powder-like and/or confluent calcific deposits together with two or more destructive lesions (vK4) [11].

Simultaneous High-Resolution Scanning X-Ray Fluorescence and Diffraction Analysis

For simultaneous high-resolution X-ray fluorescence and diffraction analysis performed at the ESRF, unstained and undecalcified sections (4 μm) were used. Sections were mounted on frames with a 1.4-μm polyethylene-naphthalene membrane (MMI slides; Olympus, Hamburg, Germany) and subsequently deparaffinized. These sections were sequential to those used for von Kossa staining. Areas with powder-like calcification (microcalcification, vK1) rather than firm calcific deposits were selected. Per sample, one region of interest (ROI) containing microcalcification was identified (see Fig. 1 for illustration of this approach). A nanofocus monochromatic X-ray beam (beamline ID 13) with 12.5 keV was used for line scanning (steps of 250 nm). Per ROI, at least one line scan with simultaneous recording of the calcium-specific X-ray fluorescence ($K_\alpha = 3.69$ keV, $K_\beta = 4.01$ keV) signals and diffractograms was performed. The latter were recorded with a two-dimensional "fast readout low noise," CCD-based diffraction camera. At each point during a scan, signals were sampled for a period of 4 seconds. Synthetic apatite, $Ca_{10}(PO_4)_6(OH)_2$, and whitlockite, $(Ca, Mg)_3(PO_4)_2$, served as positive controls and aluminium oxide, Al_2O_3, was used as a calibrator. X-ray diffraction images were integrated to the d-spacing format (d = interplanar or interatomic distance) with the software package FIT2D [24]. Background correction was applied to the integrated X-ray diffraction spectra prior to comparison with reference spectra for identification of the mineral phase. The length of tissue containing calcium phosphate (either amorphous or crystalline), whitlockite, or a mixture of both minerals at the same spot was used as a surrogate marker for the amount.

Statistical Analysis

All data were stored and analyzed using the SPSS statistical package 17.0 (SPSS, Inc., Chicago, IL). The statistics computed included mean, median, minimum, maximum, and standard errors (SEM) of continuous variables. Differences in continuous variables between two study groups were determined by the two-sample t test for independent samples or the nonparametric Mann–Whitney U test by ranks, as appropriate. Test selection was based on evaluating the variables for normal distribution employing the Kolmogorov–Smirnov test. For categorical variables, comparisons were done using the chi-squared test (Fisher′s exact test). All p values resulted from two-sided statistical tests, and $p < 0.05$ was considered to be significant.

Results

Patient Characteristics and Biochemical Data

Approximately half of the patients presented with either normal ($n = 15$) or reduced ($n = 13$) renal function (i.e., CKD stages 2–4). Apart from renal function, the two

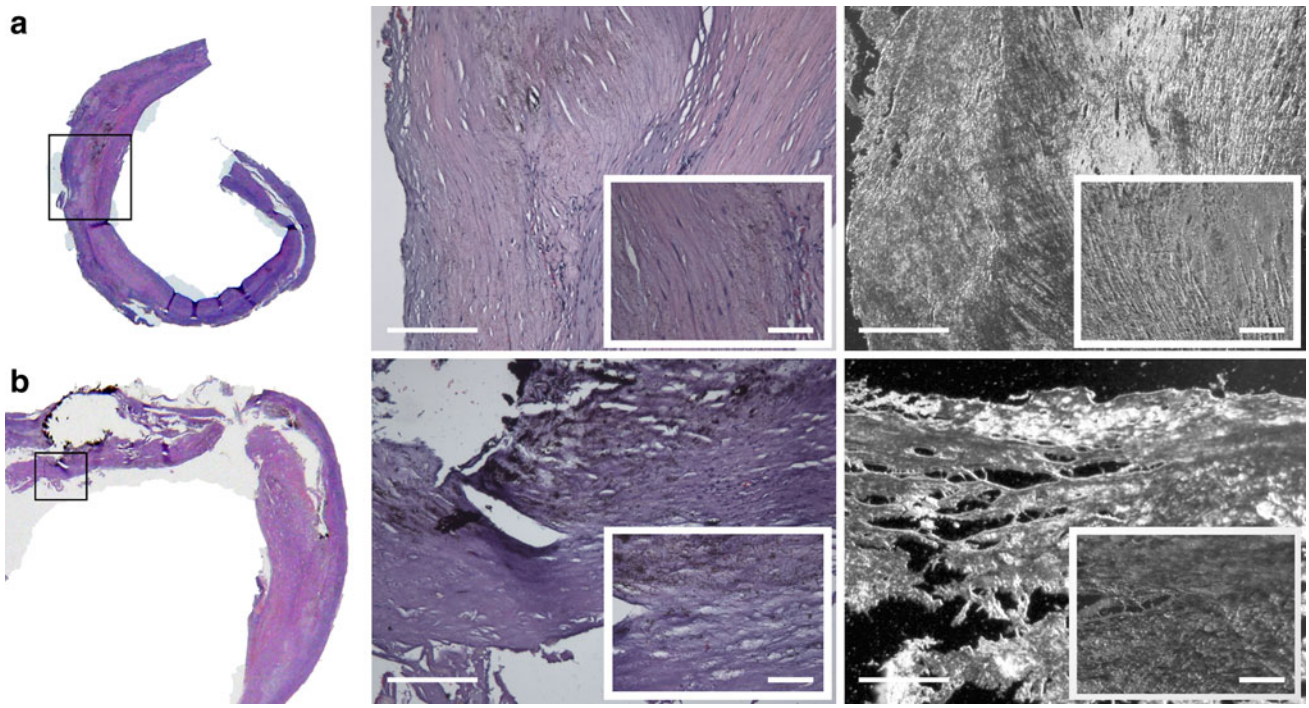

Fig. 1 Identification of microcalcification (von Kossa staining) in surgical specimens derived from atherosclerotic patients with normal renal function presenting with overall mild (vK2, **a**) or severe (vK4, **b**) calcification. The corresponding sections used for high-resolution X-ray diffraction analysis are given in the *right panel*. Regions of interest as well as lines selected for scanning analysis are indicated. Magnification: ×100, *insets* ×400

Table 2 Biochemical parameters of mineral metabolism in atherosclerotic patients with normal or reduced renal function at time of surgery

Parameter	Normal renal function	CKD stages 2–4	*p*
Magnesium (mmol/l)	1.02 ± 0.05	0.92 ± 0.09	0.525
Calcium (mmol/l)	2.27 ± 0.033	2.23 ± 0.02	0.363
Phosphate (mmol/l)	0.99 ± 0.033	0.94 ± 0.05	0.387
Ca × P ($mmol^2/l^2$)	2.25 ± 0.086	2.10 ± 0.12	0.274
PTH (pg/ml)	39.80 ± 5.33	51.70 ± 9.4	0.160
25-hydroxyvitamin D (nmol/l)	21.90 ± 3.93	32.00 ± 4.16	0.089
1,25-dihydroxyvitamin D (pg/ml)	36.20 ± 7.07	23.00 ± 3.24	0.060
cFGF-23 (RU/ml)	51.00 ± 13.8	66.00 ± 22.2	0.751
Fetuin-A (g/l)	0.38 ± 0.02	0.39 ± 0.02	0.892

Values are given as mean ± SEM and represent the concentration in plasma (cFGF-23) and serum (all other parameters)

groups did not differ significantly with respect to age, body mass index (BMI), and the frequency of established risk factors for atherosclerosis, i.e., hypertension, dyslipidemia, diabetes, and smoking history (Table 1). Compared to patients with normal renal function, CKD patients tended to present with elevated parathyroid hormone (PTH) and reduced calcitriol levels (Table 2). All patients exhibited vitamin D deficiency; i.e., the serum concentrations of 25-hydroxyvitamin D_3 (25OHD) were clearly below 75 nmol/l and severe vitamin deficiency (< 25 nmol/l) was seen in eight and four patients with normal and impaired renal function, respectively.

Histological Characterization of Tissue Samples

Calcific deposits were readily detectable in all samples, albeit of variable intensity and degree. While all except one sample derived from patients with normal renal function had to be classified as vK3 or vK4, this was seen only in eight out of 13 samples taken from CKD patients (3.4 ± 0.16 vs. 2.54 ± 0.29, $p < 0.05$). Despite these differences with respect to the overall calcification score, areas with microcalcification were present even in specimens with large calcific deposits, and these regions were selected for high-resolution scanning X-ray diffraction analysis at the ESRF (Fig. 1).

Analysis of X-Ray Diffraction Data

Per sample, at least one ROI was identified and one or more line scans with simultaneous recording of the calcium-specific X-ray fluorescence and X-ray diffraction signals were performed (Fig. 2). The total length of tissue investigated was 4,205 µm (28 samples), and comparable lengths of tissue per group and per sample were analyzed (Table 3). However, the signal intensity was too low in three samples, which were taken from two patients with normal and from one patient with impaired renal function. Consequently, these samples were excluded from the subsequent analysis. Regardless of this, the size (length) of tissue giving rise to simultaneous X-ray fluorescence signals and X-ray diffractograms ("informative samples") as well as the number of mineralized spots (19 vs. 18) were

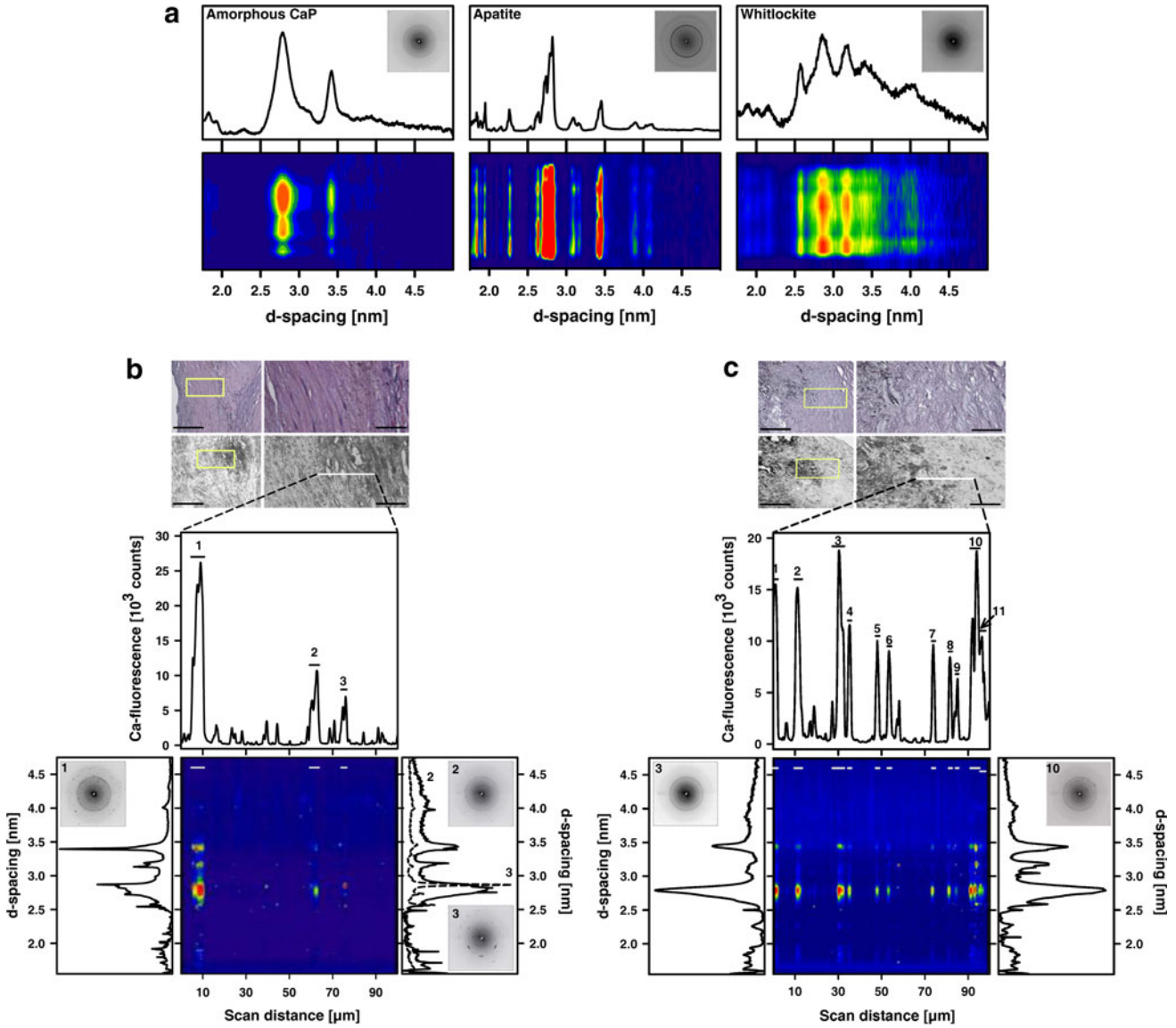

Fig. 2 High-resolution scanning X-ray fluorescence and diffraction analysis of synthetic standards (**a**) and powder-like calcification in surgical specimens derived from atherosclerotic patients with normal (**b**) and impaired (**c**) renal function. **a** Typical diffractograms (*insets*) of amorphous calcium phosphate (*left panel*), apatite (*middle panel*), and whitlockite (*right panel*). On a line scan through the standard, 35 diffractograms were collected and integrated. The corresponding d-spacing signals are shown in the line graphs. **b**, **c** *Photographs* von Kossa-stained section and corresponding unstained section used for X-ray fluorescence and diffraction analysis. The region where the line scan was taken is indicated. *Middle panel* calcium content over the line scan. *Bottom center* circular integration of the diffractograms taken at each pixel in the line scan. Regions corresponding to a high calcium content are indicated. *Bottom left and right* Typical diffractogram obtained in the indicated calcium-rich region and integrated signal. Diffraction patterns corresponding to the peaks indicated (i.e., peaks 1–3 in **b** and peaks 3 and 10 in **c**) correspond to a mixture of calcium phosphate and whitlockite (peaks 1–3 in **b** and peak 10 in **c**) and to amorphous calcium phosphate (peak 3 in **c**)

Table 3 Summary of high-resolution scanning X-ray diffraction analysis

	Normal renal function	CKD stages 2–4	*p*
Number of samples/informative samples/identified spots	15/13/19	13/12/18	
Scan data			
Total length of scanned region (μm)	2,155	2,050	0.316
Mean length ± SEM of scanned region (μm/sample)	144 ± 21.9	158 ± 36.6	
Total length of informative regions (μm)	201.00	232.00	0.574
Mean length ± SEM of informative regions (μm/sample)	15.5 ± 2.91	19.3 ± 8.44	
Total length (percentage) corresponding to			
Calcium phosphate (amorphous or crystaline) (μm)	79.0 (39 %)	157 (68 %)	<0.001
Whitlockite (μm)	94.1 (47 %)	38.7 (17 %)	< 0.001
Mixture at the same spot (μm)	27.8 (14 %)	36.3 (15 %)	0.007

Per group, the number of scanned and informative samples as well as the number of informative spots are given. The total length of scanned tissue and the total length of informative regions per group were calculated. For either mineral phase, i.e., calcium phosphate (regardless of modification), whitlockite, or a mixture of both, the total length as the sum of all spots containing this particular phase was calculated

similar in the two groups (Table 3; Figs. 1, 2). Only one type of mineral was seen in nine out of 13 samples taken from patients with normal GFR and in eight out of 12 samples derived from CKD patients. In particular, calcium phosphate (whether amorphous or crystalline), calcium/magnesium phosphate (whitlockite), or a mixture of the two at the same spot were identified, respectively, in 7 versus 7, 7 versus 8, and 5 versus 3 spots in samples derived from patients with normal versus reduced GFR. Thus, the results obtained in both groups are almost identical with respect to the number of samples and the frequency of either mineral. Since comparable regions were selected containing small powder-like calcification rather than a firm and established calcification, the mean length per mineralized spot was calculated for each group. The mean total lengths of tissue covered with either calcium phosphate (11.3 ± 4.9 vs. 22.4 ± 12.1 μm) or a mixed mineral phase (5.6 ± 1.1 vs. 12.1 ± 3.9 μm) did not differ significantly between groups. By contrast, in samples derived from patients with normal renal function the mean length of tissue covered with whitlockite was significantly larger compared to patients with impaired renal function (13.4 ± 2.9 vs. 4.8 ± 1.4 μm, $p < 0.05$).

While the set of data reported above is related to the number of samples from either group, we summarized the informative regions in all samples per group into one composite sample and compared these with respect to the total length of tissue mineralized with either calcium phosphate or whitlockite (Table 3). Whereas in the composite sample corresponding to patients with normal renal function, whitlockite and calcium phosphate contribute to the mineral phase to an almost identical extent, approximately two-thirds of the mineral consists of calcium phosphate in the patients with impaired renal function. The total length of tissue covered with either whitlockite or calcium phosphate differed significantly between the two groups (Table 3). Indeed, while whitlockite is in excess in patients with normal renal function, calcium phosphate (either amorphous or in the form of apatite) is most prevalent in samples from patients with impaired renal function (each $p < 0.001$, Table 3).

Discussion

It is widely accepted that vascular calcification, in the form of either "classical" or uremia-associated atherosclerosis, is a highly regulated process, closely resembling skeletal mineralization and ossification [2]. Multiple cellular and molecular processes required to transfer a nonmineralizable matrix into a mineralizable one have been indentified [4, 7, 25]. By contrast, little information on the physicochemical properties of microcalcification, i.e., those dispersed throughout the extracellular matrix of the aortic tunica media, is available. Instead, it is widely assumed that the minerals deposited in vessels and bone are largely identical, i.e., carbonate apatite as the main mineral phase. However, the occurrence of apatite represents the end rather than the beginning of the mineralization process. In fact, amorphous calcium phosphate has been described at the edges of overall advanced calcific deposits, i.e., apatite crystals, in the aortic tunica media [18]. Those edges represent the "invasion front" of an invasive calcification rather than the starting point of an entirely new calcific deposit.

We attempted to gain knowledge on the ultrastructural properties and composition of microcalcifications, although surgical specimens with only microcalcification in arteries are rare. Therefore, we used tissue specimens from patients undergoing carotid endarterectomy for severe

atherosclerosis. These patients present with either normal or reduced renal function (CKD stages 2–4). Irrespective of the extension and degree of atherosclerosis, microcalcifications were dispersed throughout the media of the carotid artery, and those fairly distant from large destructive calcification were investigated with high-resolution X-ray diffraction analysis. The probe size of 250 × 250 nm allowed us to resolve the structure of these microdeposits at a submicrometer scale. To the best of our knowledge, this is the first study comparing the frequency and relative contribution of whitlockite and calcium phosphate to microcalcification in patients with normal and moderately impaired renal function. This approach revealed that (1) in microcalcification most of the calcium phosphate was amorphous rather than mature apatite and (2) the relative contributions of whitlockite and calcium phosphate to microcalcification differed between patients with normal and mildly impaired renal function.

Although the frequency of either mineral phase did not differ between groups, their relative contribution to the mineral composition of the microcalcification per group was significantly different. Indeed, comparison of patients with normal vs. reduced renal function (CKD stages 2–4) revealed a significantly larger proportion of the microcalcification to consist of whitlockite and apatite in the former group. While whitlockite is not an entirely newly identified component of pathological calcification, the significance of this finding is still a matter of discussion [18–21, 26]. This may, at least in part, be due to the fact that whitlockite and calcium phosphate cannot be reliably discriminated using routine histological techniques including sensitive silver staining according to von Kossa [26]. Instead, other methods, like Raman spectroscopy or X-ray diffraction analysis, are required to resolve the crystallographic properties associated with the different mineral phases.

The presence of whitlockite within ectopic calcifications may be more than merely an "academic" finding, although both whitlockite and apatite are equally insoluble and represent a state of irreversible mineralization [27]. Rather, the presence of whitlockite points to distinct differences in the local environment and especially the local magnesium concentration at the time of mineralization rather than the systemic magnesium concentration at the time of sampling [20]. This point of view concurs with the fact that in our study serum magnesium concentrations did not significantly differ in patients with normal or reduced GFR at the time of surgery. An aberrant vitamin D/mineral metabolism has been thought to contribute to (ectopic) vascular calcification, and the therapeutic window for treatment with active vitamin D (calcitriol) appears to be narrow [28–30]. Regardless of this, serum parameters of mineral metabolism were quite comparable in patients with normal renal function and mild CKD. Recently, a negative association between 25OHD levels and the progression of coronary artery calcification has been shown in patients with normal and reduced renal function, and this may also be a contributing factor to the findings of the present study [31]. Again, it must be considered that vitamin D levels were determined at the time of vascular surgery, i.e., when formation of microcalcification was already completed. Thus, it is difficult to link these two observations in a causative manner. Moreover, all patients were vitamin D-deficient, and the distinct relative distribution of calcium phosphate and whitlockite throughout the samples derived from patients with normal and reduced renal function was independent of vitamin D status.

In uremic rats severe media calcification can be induced by a high phosphate intake and/or calcitriol loading [18, 23, 32]. Interestingly, whitlockite was primarily seen after high-dose calcitriol treatment rather than phosphate loading alone. It has been suggested that calcitriol stimulates the formation of whitlockite by enhancing gastrointestinal magnesium absorption [18]. If the suggested association between vitamin D-stimulated magnesium absorption and formation of whitlockite also holds true in humans, the presence of whitlockite in our set of samples reflects local magnesium balance at the time of microcalcification. Unfortunately, it is not possible to assess the course of vascular calcification from human samples as these are related to a clinically defined end point rather than to the time required for progression to this end point.

The present study has several limitations. The applied procedures for fixation and processing of tissue may raise concerns regarding the stability of the microcalcifications, especially with respect to kinetically unstable amorphous calcium phosphate [17]. Although more sophisticated protocols directed at stabilizing the native structure of the tissue and reducing fixation-related artifacts are available, these are hardly feasible for sampling of human tissue during surgery [17, 33]. Moreover, our approach has previously been used successfully by us and other groups [18, 21]. The total number of samples as well as the investigated length of tissue per sample are rather small (a limitation which is mainly due to the requested/allowed beam time for synchrotron-based X-ray microdiffraction). Therefore, we cannot exclude that factors other than renal function (e.g., gender, age, diabetes) are relevant to the mineral composition.

In summary, we have shown that arterial microcalcification in atherosclerotic patients with normal or reduced renal function consists of calcium phosphate (either amorphous or in the form of apatite) and whitlockite. While the frequency of either mineral phase did not differ between groups, the relative contribution of whitlockite was significantly greater in patients with normal renal function. Chronic impairment of renal function may significantly

affect local magnesium homeostasis, with the latter being reflected in the physicochemical composition of microcalcification in atherosclerotic patients.

Acknowledgments The outstanding technical assistance of Birgit Salewski and Anja Rahn is highly appreciated. We acknowledge the European Synchrotron Radiation Facility for provision of synchrotron radiation facilities and for assistance in using beamline ID 13. The study was funded by a grant (FORUN-program, 88 90 47) from the Medical Faculty, University of Rostock.

References

1. Rennenberg RJ, Kessels AG, Schurgers LJ, van Engelshoven JM, de Leeuw PW, Kroon AA (2009) Vascular calcifications as a marker of increased cardiovascular risk: a meta-analysis. Vasc Health Risk Manag 5:185–197
2. Persy V, D'Haese P (2009) Vascular calcification and bone disease: the calcification paradox. Trends Mol Med 15:405–416
3. Atkinson J (2008) Age-related medial elastocalcinosis in arteries: mechanisms, animal models, and physiological consequences. J Appl Physiol 105:1643–1651
4. Abedin M, Tintut Y, Demer LL (2004) Vascular calcification: mechanisms and clinical ramifications. Arterioscler Thromb Vasc Biol 24:1161–1170
5. Dellegrottaglie S, Sanz J, Rajagopalan S (2006) Molecular determinants of vascular calcification: a bench to bedside view. Curr Mol Med 6:515–524
6. O'Neill WC, Lomashvili KA (2010) Recent progress in the treatment of vascular calcification. Kidney Int 78:1232–1239
7. Demer LL, Tintut Y (2008) Vascular calcification: pathobiology of a multifaceted disease. Circulation 117:2938–2948
8. Speer MY, Giachelli CM (2004) Regulation of cardiovascular calcification. Cardiovasc Pathol 13:63–70
9. Shao JS, Cai J, Towler DA (2006) Molecular mechanisms of vascular calcification: lessons learned from the aorta. Arterioscler Thromb Vasc Biol 26:1423–1430
10. Shao JS, Cheng SL, Sadhu J, Towler DA (2010) Inflammation and the osteogenic regulation of vascular calcification: a review and perspective. Hypertension 55:579–592
11. Voigt M, Fischer DC, Rimpau M, Schareck W, Haffner D (2010) Fibroblast growth factor (FGF)-23 and fetuin-A in calcified carotid atheroma. Histopathology 56:775–788
12. Bobryshev YV (2005) Transdifferentiation of smooth muscle cells into chondrocytes in atherosclerotic arteries in situ: implications for diffuse intimal calcification. J Pathol 205:641–650
13. Neven E, Dauwe S, De Broe ME, D'Haese PC, Persy V (2007) Endochondral bone formation is involved in media calcification in rats and in men. Kidney Int 72:574–581
14. Jahnen-Dechent W, Heiss A, Schäfer C, Ketteler M (2011) Fetuin-a regulation of calcified matrix metabolism. Circ Res 108:1494–1509
15. Vattikuti R, Towler DA (2004) Osteogenic regulation of vascular calcification: an early perspective. Am J Physiol Endocrinol Metab 286:E686–E696
16. Toussaint ND (2011) Extracellular matrix calcification in chronic kidney disease. Curr Opin Nephrol Hypertens 20:360–368
17. Wuthier RE, Lipscomb GF (2011) Matrix vesicles: structure, composition, formation and function in calcification. Front Biosci 17:2812–2902
18. Verberckmoes SC, Persy V, Behets GJ, Neven E, Hufkens A, Zebger-Gong H, Muller D, Haffner D, Querfeld U, Bohic S, De Broe ME, D'Haese PC (2007) Uremia-related vascular calcification: more than apatite deposition. Kidney Int 71:298–303
19. LeGeros RZ, Contiguglia SR, Alfrey AC (1973) Pathological calcifications associated with uremia: two types of calcium phosphate deposits. Calcif Tissue Res 13:173–185
20. Lagier R, Baud CA (2003) Magnesium whitlockite, a calcium phosphate crystal of special interest in pathology. Pathol Res Pract 199:329–335
21. Schlieper G, Aretz A, Verberckmoes SC, Krüger T, Behets GJ, Ghadimi R, Weirich TE, Rohrmann D, Langer S, Tordoir JH, Amann K, Westenfeld R, Brandenburg VM, D'Haese PC, Mayer J, Ketteler M, McKee MD, Floege J (2010) Ultrastructural analysis of vascular calcifications in uremia. J Am Soc Nephrol 21:689–696
22. Levey AS, Bosch JP, Lewis JB, Greene T, Rogers N, Roth D (1999) A more accurate method to estimate glomerular filtration rate from serum creatinine: a new prediction equation. Modification of diet in Renal Disease Study Group. Ann Intern Med 130:461–470
23. Haffner D, Hocher B, Muller D, Simon K, Konig K, Richter CM, Eggert B, Schwarz J, Godes M, Nissel R, Querfeld U (2005) Systemic cardiovascular disease in uremic rats induced by $1,25(OH)_2D_3$. J Hypertens 23:1067–1075
24. Hammersley AP, Svensson SO, Hanfland M, Fitch AN, Hausermann D (1996) Two-dimensional detector software: from real detector to idealised image or two-theta scan. High Press Res 14:235
25. Murshed M, McKee MD (2010) Molecular determinants of extracellular matrix mineralization in bone and blood vessels. Curr Opin Nephrol Hypertens 19:359–365
26. Reid JD, Andersen ME (1993) Medial calcification (whitlockite) in the aorta. Atherosclerosis 101:213–224
27. O'Neill WC (2007) Vascular calcification: not so crystal clear. Kidney Int 71:282–283
28. Zittermann A, Schleithoff SS, Koerfer R (2007) Vitamin D and vascular calcification. Curr Opin Lipidol 18:41–46
29. Shroff R, Knott C, Rees L (2010) The virtues of vitamin D–but how much is too much? Pediatr Nephrol 25:1607–1620
30. Razzaque MS (2011) The dualistic role of vitamin D in vascular calcifications. Kidney Int 79:708–714
31. de Boer IH, Kestenbaum B, Shoben AB, Michos ED, Sarnak MJ, Siscovick DS (2009) 25-Hydroxyvitamin D levels inversely associate with risk for developing coronary artery calcification. J Am Soc Nephrol 20:1805–1812
32. Lopez I, Mendoza FJ, Aguilera-Tejero E, Perez J, Guerrero F, Martin D, Rodriguez M (2008) The effect of calcitriol, paricalcitol, and a calcimimetic on extraosseous calcifications in uremic rats. Kidney Int 73:300–307
33. Arsenault AL, Ottensmeyer FP, Heath IB (1988) An electron microscopic and spectroscopic study of murine epiphyseal cartilage: analysis of fine structure and matrix vesicles preserved by slam freezing and freeze substitution. J Ultrastruct Mol Struct Res 98:32–47